Acridone-Amine D-A-D Thermally Activated Delayed Fluorescence Emitters With Narrow Resolved Electroluminescence and Their Electrochromic Properties

Marharyta Vasylieva [a,b], Piotr Pander *[,c], Bharat K. Sharma [d], Azam M. Shaikh [d], Rajesh M. Kamble *[,d], Fernando B. Dias [c], Malgorzata Czichy [a], Przemyslaw Data *[,a,b,1]

[a] *Faculty of Chemistry, Silesian University of Technology, M. Strzody 9, 44-100 Gliwice, Poland*

[b] *Centre of Polymer and Carbon Materials of the Polish Academy of Sciences, ul. M. Curie-Skłodowskiej 34, 41-819, Zabrze, Poland*

[c] *Department of Physics, University of Durham, South Road, Durham DH1 3LE, United Kingdom*

[d] *Department of Chemistry, University of Mumbai, Mumbai, 400 098, India*

E-mail:
Dr Piotr Pander, piotr.h.pander@durham.ac.uk;
Dr Rajesh M. Kamble, kamblerm@chem.mu.ac.in;
Prof. Przemyslaw Data, przemyslaw.data@polsl.pl.

Abstract

Acridones have found their role in luminescent materials for OLEDs. Most interestingly, showing potential as weak charge transfer thermally activated delayed fluorescence (TADF) emitters, providing narrow photoluminescence. In this work, we present a comprehensive study of donor-acceptor-donor (D-A-D) acridone-amine derivatives showing TADF and UV electrochromic properties. Structure-property relationships are studied using electrochemical and spectroelectrochemical methods as well as using photophysical characterization. Most successful emitters are used as luminescent materials in OLED, showing narrow (FWHM = 66-85 nm) electroluminescence in the green region with maximum EQE = 5.4%.

Keywords

Acridone; spectroelectrochemistry; electron paramagnetic resonance; OLED; TADF

[1] ISE member

1 Introduction

Increased interest in the more rational use of energy sources has stimulated the development of new technologies, such as organic light-emitting diode (OLED) devices.[1] One of the aims of OLED research is the selection of materials that could be used as the emitter in the active layer of such devices.[2–6] There are a plethora of molecular design strategies established to improve the performance of such devices. These are aimed, among other things, at increasing their photoluminescence quantum yield (Φ_{PL}), improving solubility and charge-transport properties, and finally at achieving efficient triplet harvesting. Emitters showing effective triplet-harvesting have found a profound role in OLEDs as emitters and hosts.[7,8] It is because these types of emissive systems provide up to 100% exciton extraction in OLED devices.[9,10] The most common examples are metal-free thermally activated delayed fluorescence (TADF) emitters[11–16] and organometallic phosphorescent complexes.[2,6,17–19] However, metal-based compounds are not always desirable. Their usage in the displays and lighting, for example, may create additional problems due to the scarcity and large cost of heavy metals, such as iridium or platinum. Therefore, many turn their attention towards metal-free emitters showing TADF. The most common design pattern of these emitters is the donor-acceptor structure. This may appear in structures with various numbers of donors (D) and acceptors (A), but the most common are simple D-A (one donor, one acceptor) or D-A-D (two donors, one acceptor). The latter is explored in this work.

Donor-acceptor systems provide an easy way to reach the synthetic goal using existing libraries of donors and acceptors. The properties of these systems can be easily tuned by using various known donors with a new acceptor or *vice versa*. One of the broadly available and low-cost acceptors is the 9(10*H*)-acridanone (acridone). It has shown great feasibility to be used in blue TADF D-A-D emitters, showing narrow emission[20] and generally in other D-A-D or D-A luminophores as an acceptor.[21–23] Acridone is also used as an acceptor in other, i.e. non-luminescent systems, such as electrodeposited films, due to the formation of a stable radical anion upon reduction.[24] Acridone skeleton has also been found in bioactive molecules.[25]

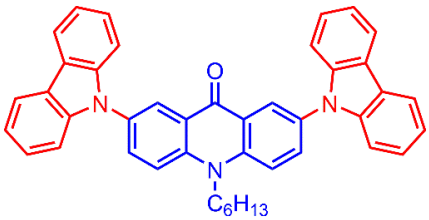

BCbAc

Scheme 1. Structure of the blue TADF emitter based on acridone acceptor.[20]

One of the disadvantages of donor-acceptor emitters for application in displays is their extensively broad luminescence spectrum, which creates difficulties to achieve good color purity.[12,26,27] Therefore, efforts are being a pursuit to design systems with a sufficiently narrow emission spectrum to improve their potential use in OLED displays,[28] where narrow emission is crucial for proper color representation. The previously presented blue TADF **BCbAc** (Scheme 1) has shown narrow luminescence, thus indicating a strong potential to explore this property in other colors. With this aim, we decided to investigate molecules **1**−**4** (Scheme 2) to develop green emitters with narrow emission spectra.[29]

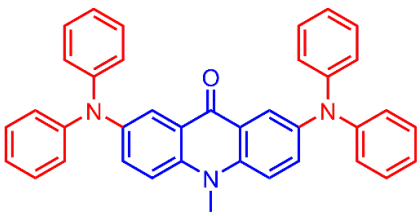

1

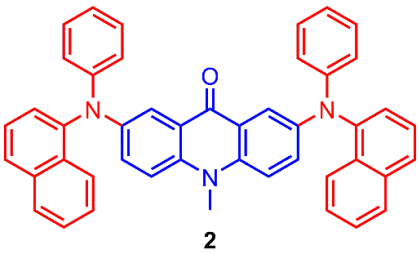

2

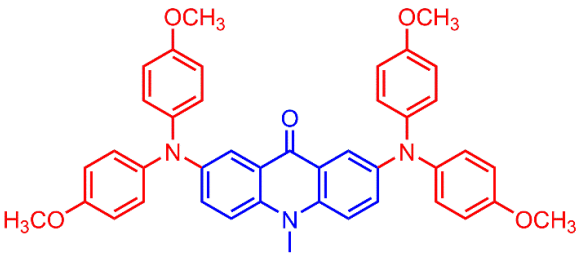

3

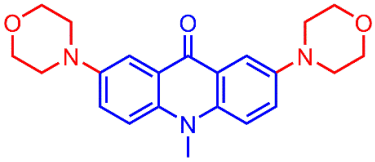

4

Scheme 2. Structures of acridone-amine D-A-D molecules investigated in this work.[29] Note the acceptor is presented in blue and the donors in red.

2 Experimental

General. All the reagents were purchased from commercial sources (Sigma Aldrich and Alfa Aesar) and were used without any further purification. The organic solvents were of analytical or spectroscopic grade and were dried and freshly distilled using the standard procedures whenever anhydrous solvents were required. ^{1}H-NMR (300 MHz) and ^{13}C-NMR (75 MHz) spectra were recorded on a Bruker 300 Ultrashield spectrometer with tetramethylsilane (TMS) as an internal reference and residual $CHCl_3$ in $CDCl_3$ as reference. Fourier transform infrared (FT-IR) spectra were recorded on a Perkin Elmer Frontier 91579. Mass spectrometric measurements were recorded using MALDI-TOF (Bruker). Melting points of the products were determined by the open capillary method.

General synthesis. The synthetic route for the target compounds **1**−**4** is described in the Supporting Information. The synthetic procedures used follow the ones described in our earlier work.[29]

Materials. Electrochemical measurements were conducted at 0.5 mM concentration (cyclic voltammetry measurements). In UV-Vis-NIR and Electron Spin Resonance (ESR) spectroscopy a higher concentration of 1.5 mM was used. Electrochemical studies were conducted in 0.1 M solutions of supporting electrolyte Bu_4NBF_4, 99% (Sigma Aldrich) in dichloromethane (DCM), CHROMASOLV1, 99.9% (Sigma Aldrich) at room temperature. UV-Vis spectroelectrochemical measurements were performed on the ITO (Indium Tin Oxide) quartz glass working electrode.

Electrochemistry and spectroelectrochemistry. Electrochemical investigation was carried out using a CHInstruments660 potentiostat. The electrochemical cell comprised of the platinum electrode with a 1 mm diameter disc as a working electrode for electrochemical measurements and ITO glass as a working electrode for spectroelectrochemical studies, Ag/AgCl electrode as a reference electrode, and platinum coil as an auxiliary electrode. Cyclic voltammetry measurements were conducted at room temperature at a scan rate of 50 mV/s. The working electrode potential was calibrated against ferrocene/ferrocenium redox couple. UV-Vis-NIR spectroscopy and spectroelectrochemistry were performed using an Ocean Optics QE6500 and NIRQuest matrix

spectrometers. In situ EPR spectroelectrochemical experiments were undertaken using a JES-FA 200 (JEOL) spectrometer.

Calculations. DFT calculations were performed using Orca 4.2.1 software[30,31] and visualized using Gabedit 2.5.1[32]. Ground state geometry and molecular orbital (MO) isosurfaces were calculated using B3LYP[33,34] functional and 6-31G(d)[35] basis set and a Conductor-like Polarizable Continuum Model (CPCM) solvent model (CH_2Cl_2).

Photophysics. Absorption spectra in solutions were recorded with a UV-3600 double beam spectrophotometer (Shimadzu). Photoluminescence (PL) spectra in solutions and films were recorded using FluoroMax-3 or FluoroLog fluorescence spectrometer (Jobin Yvon). Phosphorescence, prompt fluorescence (PF), and delayed fluorescence (DF) spectra and fluorescence decay traces were recorded using nanosecond gated luminescence and lifetime measurements (from 400 ps to 1 s) using either third harmonics of high energy pulsed Nd: YAG laser at 355 nm (EKSPLA) or an N_2 laser at 337 nm. Emission was focused onto a spectrograph and detected on a sensitive gated iCCD camera (Stanford Computer Optics) having sub-nanosecond temporal resolution. PF/DF time-resolved measurements were performed by exponentially increasing gate and integration times. Temperature-dependent experiments were conducted using a liquid nitrogen cryostat (Janis Research) under nitrogen atmosphere, while measurements at room temperature were recorded in a vacuum in the same cryostat. Power dependence results were fitted using the expression $y = a \cdot x$ for linear, proportional relation. Details of the iCCD setup and measurements can be found elsewhere.[36]

OLED devices. OLEDs were fabricated with vacuum thermal evaporation. Devices of 4x2 mm pixel size were fabricated. HAT-CN – dipyrazino[2,3-*f* :2',3'-*h*]quinoxaline-2,3,6,7,10,11-hexacarbonitrile (LUMTEC), PO-T2T – 2,4,6-Tris[3-(diphenylphosphinyl)phenyl]-1,3,5-triazine (LUMTEC), mCP – 1,3-Bis(carbazol-9-yl)benzene (LUMTEC), NPB - *N*,*N*′-di(1-naphthyl)-*N*,*N*′-diphenyl-(1,1′-biphenyl)-4,4′-diamine (LUMTEC), TSBPA (4,4'-(diphenylsilanediyl)bis(*N*,*N*-diphenylaniline)), TPBi - 2,2′,2″-(1,3,5-benzinetriyl)-tris(1-phenyl-1*H*-benzimidazole) (LUMTEC), CBP - 4,4′-bis(*N*-

carbazolyl)-1,1′-biphenyl (LUMTEC), LiF (99.995%, Sigma Aldrich), and Aluminium wire (99.9995%, Alfa Aesar) were purchased from the companies indicated in parentheses. NPB was used as a hole transport layer (HTL), while TSBPA played the role of an electron blocking layer and an additional hole transport layer to step-up the HOMO energy and reduce the injection barrier to CBP. HAT-CN was used as a hole injection layer. TPBi or PO-T2T were used as an electron transport layer (ETL), while CBP or mCP were used as a host material. OLED devices were fabricated using pre-cleaned with ozone plasma indium-tin-oxide (ITO) coated glass substrates with a sheet resistance of 20 Ω cm^{-2} and ITO thickness of 100 nm. All organic and inorganic layers were thermally evaporated using Kurt J. Lesker Spectros II deposition system at 10^{-6} mbar. All organic materials and aluminum were deposited at a rate of 1 Å s^{-1}. The LiF layer was deposited at a rate of 0.1-0.2 Å s^{-1}. Characterization of OLED devices was conducted in a 10-inch integrating sphere (Labsphere) connected to a Source Measure Unit and coupled with a spectrometer USB4000 (Ocean Optics). Further details can be found in the literature.[37]

3 Results and discussion

3.1 Photophysics in solution

The molecules presented in this work belong to the same structural group of D-A-D compounds sharing a common acceptor and strong similarities between donors. Therefore, it is no surprise that their absorption and emission spectra show good resemblance among the series (**Figure 1**). All compounds show green fluorescence with high to moderate photoluminescence quantum yield.[29] The absorption spectra show two general groups of absorption bands: those related to charge transfer (CT) transitions and those related to π-π* transitions (**Figure 2** and S1). The CT absorption bands clearly show a lower absorption coefficient ≈5000 M^{-1} cm^{-1} and unequivocal positive solvatochromism which is a sign of a charge transfer band involving π-π* transitions. The other group of absorption bands is associated with localized π-π* transitions. This is evidenced by their absorption coefficients ≈25000-50000 M^{-1} cm^{-1} being larger by one order of magnitude. Further to that, no

significant solvatochromic shifts are observed involving these bands. Having this established, the localized π-π* transitions are associated with absorption below 370 nm in compounds **1**−**3** and below 330 nm in **4**, while absorption bands at longer wavelengths are related to CT transitions. It is worth to mention that, most likely, the absorption bands at $\lambda_{abs} \approx 350$ nm in **1-3** are associated with the donor – this is evidenced by the lack of such band in **4**. Moreover, these bands are affected by the type of diarylamine donor in a way consistent with structure of the substituent (i.e. red shift with larger conjugation). The maximum $\lambda_{abs} = 348$ nm in **1**, for example, is subsequently red shifted in **3** to $\lambda_{abs} = 353$ nm due to the electron-donating effect of the methoxy groups. On the other hand, in **2** the band shows a shoulder at 350-400 nm – this can be associated with the absorption of the naphthylamino group in the donor.

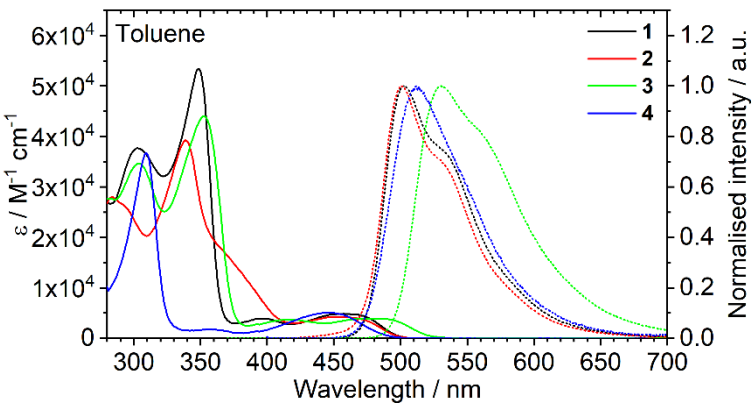

Figure 1. Absorption (continuous lines) and normalized photoluminescence (dotted lines) spectra recorded in the toluene solution.

All compounds in the series show narrow photoluminescence spectra and those of **1**−**3** group show a degree of vibronic resolution, contrary to typical spectra of D-A-D molecules with CT emissive states. However, the vibronic resolution is lost and accompanied by a pronounced redshift of the emission maxima in polar solvents (**Figure 2** and S1). This is an indication that all the molecules studied in the work show a CT excited state, but with a moderate degree of charge transfer. Compound **3** shows the most red-shifted emission $\lambda_{em} = 530$ nm in respect to **1**, $\lambda_{em} = 502$ nm, which is related to the strongest electron-donating properties of the donor in **3**. This is also evidenced by the smallest energy gap of

3. Finally, all the molecules show strong re-absorption in the high energy side of their emission spectra due to a small Stokes shift: 45-48 nm (240-260 meV) in **1** and **2**, and slightly larger in **3**, 56 nm (280 meV) and 66 nm (360 meV) in **4**.

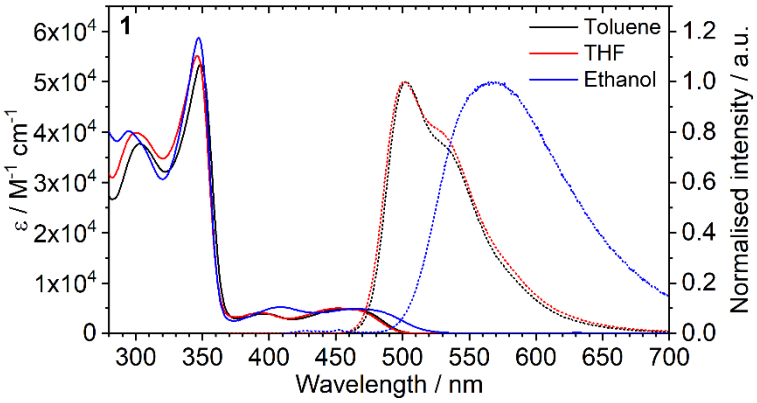

Figure 2. Absorption (continuous lines) and normalized photoluminescence (dotted lines) spectra of **1** recorded in three different solvents indicated in the figure legend.

3.2 DFT calculations

The acridone acceptor remains generally nearly planar in the ground state with either of the diphenylamino aryl groups in **1**−**3** orthogonal to the acceptor plane. The HOMO is localized not only on the donors, as typically found in D-A-D molecules with strong CT character, but shows a rather elevated contribution of the acceptor. This is an indication of a partial conjugation existing between each of donors with the acceptor as well as the donors between each other (through the acceptor). HOMO and HOMO-1 generally show symmetric geometry, suggesting that the donors are in all cases equal and processes such as excitation or one-electron oxidation should involve both moieties. LUMO's are localized on the acceptor in all cases. This renders the HOMO→LUMO transition to have a partial CT character due to generally moving the charge away from the donors and towards the acceptor in the excited state. This is consistent with the photophysical properties of these compounds as they show only a weak CT character. HOMO and LUMO energy follow the trend established in electrochemistry (Table 1) and follow the expected donor strength. The calculated values show an offset of 0.5-0.7 eV towards HOMO and 1.2-1.3 eV towards LUMO if absolute energy values are considered.

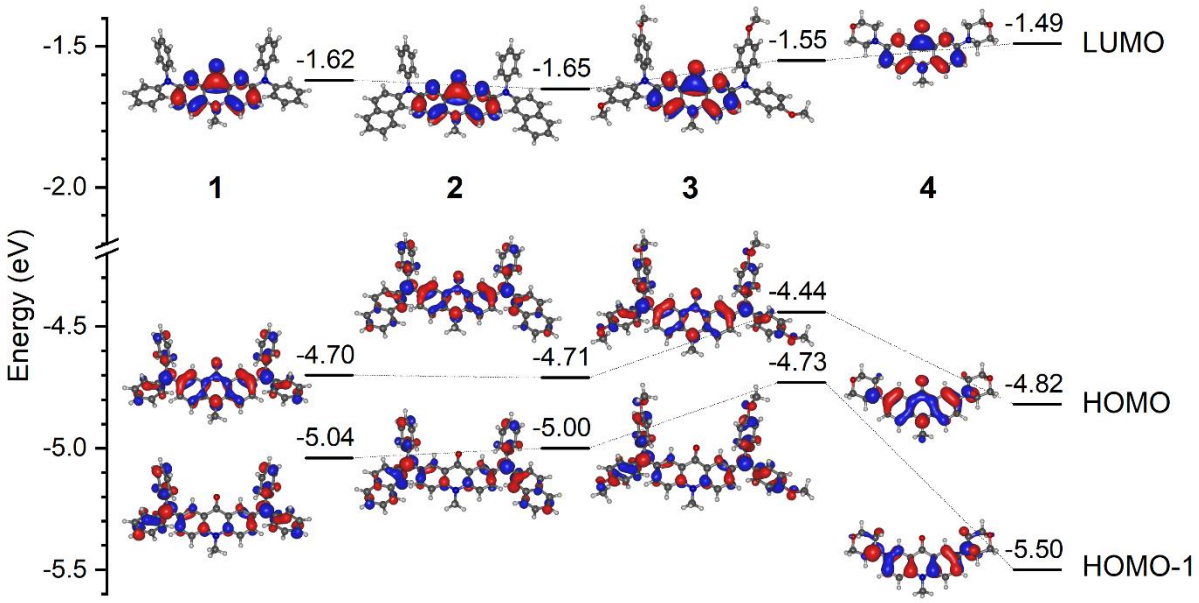

Figure 3. Molecular orbital isosurfaces and energy calculated at B3LYP/6-31g(d) level of theory with iso value of 0.03. All values are shown in eV.

3.3 Electrochemistry

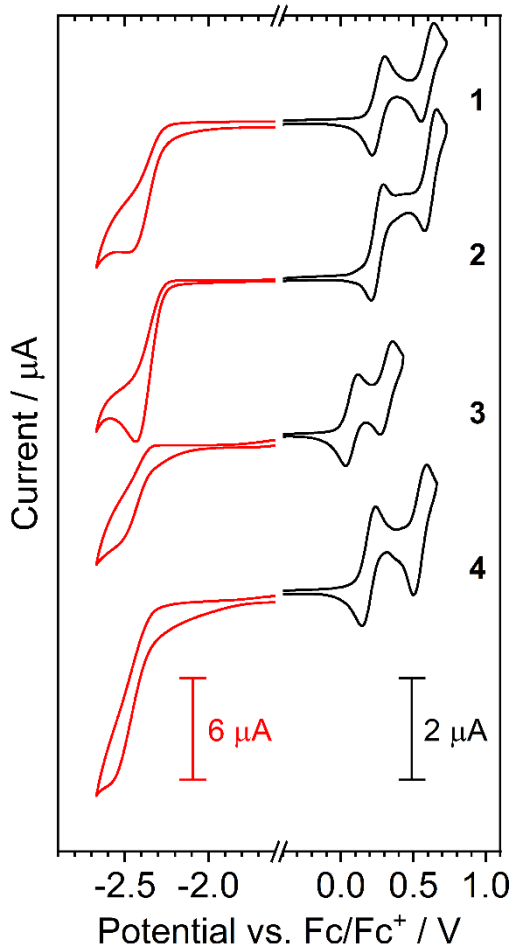

Figure 4. Electrochemical oxidation and reduction processes recorded with cyclic voltammetry in 0.1M Bu_4NBF_4 / CH_2Cl_2 supporting electrolyte. Note: the current of reduction process (red) has been scaled for clarity.

Molecules **1**−**4** all show oxidation and reduction processes in the electrochemical window of the supporting electrolyte (**Figure 4**). The first oxidation process is reversible in all cases, while all reduction processes are irreversible. The oxidation onset potential follows the expected donor strength, with the lowest observed in **3**. The methoxy substituents act as group donating electrons to the diphenylamino unit, destabilizing the HOMO. Interestingly, the naphthylamino group in **2** does not affect the oxidation potential of the molecule, which remains virtually identical to that of **1**. The reduction onset potential does not significantly change between the molecules, confirming the location of LUMO on the acceptor – this being the only common unit of all four. Each of the compounds shows two consecutive reversible oxidation processes, likely related to withdrawal of the

first and the second electron, respectively, jointly from the two donor moieties. Electrochemical properties of **1**−**4** are summarized in Table 1.

Table 1. Summary of electrochemical results and calculations.

	Cyclic voltammetry								**Calculations**			
	$E_{½}^{ox}$, V		**E_{ox}^{onset}, V**		**E_{red}^{onset}, V**	**IP, eV**	**EA, eV**	**E_g^{el}, eV**	**HOMO, eV**	**HOMO-1, eV**	**LUMO, eV**	**E_g^{calc}, eV**
	1st	2nd	1st	2nd								
1	0.26	0.60	0.19	0.54	-2.24	5.29	2.86	2.43	-4.70	-5.04	-1.62	3.08
2	0.25	0.62	0.18	0.55	-2.24	5.28	2.86	2.42	-4.71	-5.00	-1.65	3.06
3	0.08	0.31	0.00	0.26	-2.28	5.10	2.82	2.28	-4.44	-4.73	-1.55	2.89
4	0.19	0.55	0.12	0.48	-2.29	5.22	2.81	2.41	-4.82	-5.50	-1.49	3.33

3.4 Spectroelectrochemistry

Figure 5 shows the UV-Vis-NIR absorption spectra of the initial, neutral compound, and its gradual transformation into the oxidation product, a cation radical. Isosbestic points are visible in all spectra and indicated with a line at the respective absorption energy. A presence of an isosbestic point suggests that one species is transformed into another in a single process: the bands diminishing in intensity are related to the substrate and those arising are related to the product. Not surprisingly, all spectra show only one isosbestic point, which indicates a single product being formed, without further reactions or intermediates involved. All absorption bands rising at an energy below the isosbestic point are attributed to the cation radical, while all bands diminishing at energies larger than the isosbestic point are attributed to transitions within the neutral compound. Each of the radical cations shows many additional absorption bands at lower energy than the respective neutral compound, including a pronounced NIR band. Interestingly, the NIR absorption band (<1.5 eV) that is associated with each cation radical is at lower energy in **1**−**3** with arylamino donors, than in **4**, with a morpholino donor. The bands at lower energy are likely to be associated with the electron transitions from lower HOMO orbitals to the SOMO of the radical.

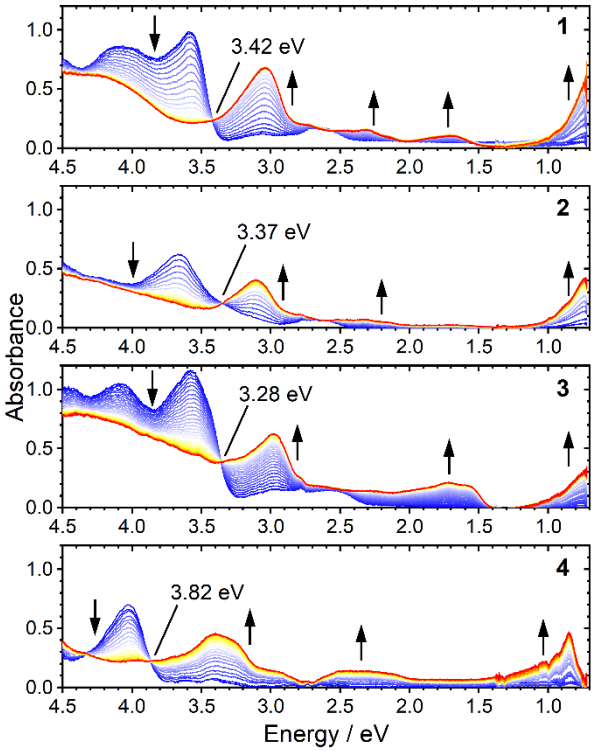

Figure 5. UV-Vis-NIR absorption spectra recorded upon *in situ* potentiostatic oxidation of **1**−**4** at the first oxidation peak potential. Each spectrum is recorded at 10 s time interval. The thicker blue line indicates the first (neutral), while the thicker red line indicates the final spectrum of the product (cation radical).

3.5 Electrochromic properties

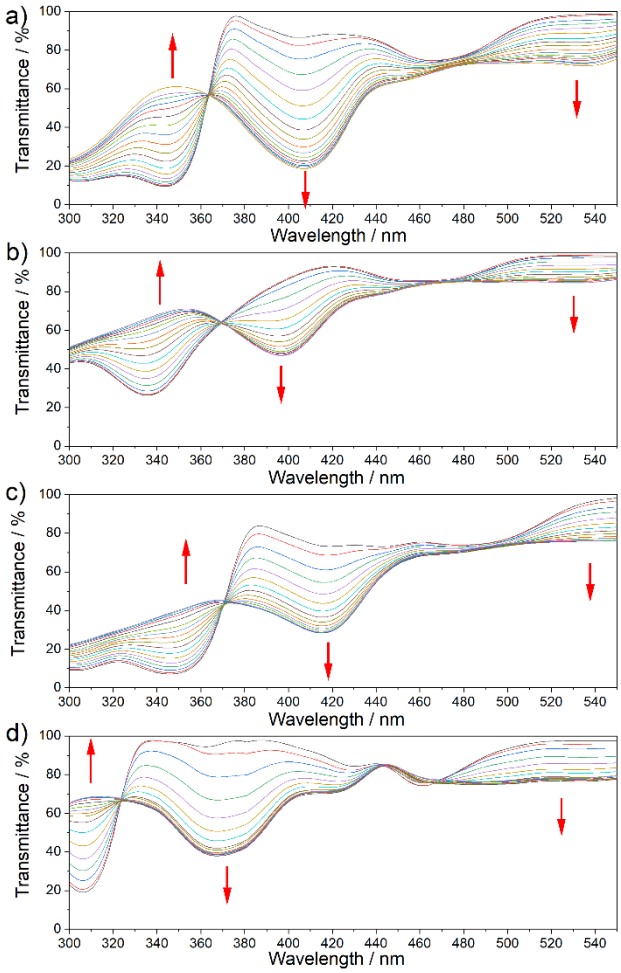

Figure 6. UV-Vis transmittance of pristine films of a) **1**, b) **2**, c) **3** and d) **4** under electrooxidation.

The analyzed compounds show very interesting active electrochromic properties in the UV region (**Figure 6**). As many light sources emit UV-A / deep blue light, devices like displays or lighting often comprise additional blue light filters. Such blue light may cause eye fatigue. In that matter, the development of novel active UV-A / deep blue filters is a very important part of organic electronic devices. In our case, the active layers were spin-coated, obtaining thickness of ca. 200 nm, and used for electrochromic characterization. In this case electrochromic behavior of two bands was studied: the π-π* absorption band of neutral compounds in UV-A (< 400 nm) and the UV (340 nm) / deep blue (400-420 nm) polaronic band. Interestingly, both of the investigated bands in compound **4** fall within the UV-A region. The best results were obtained for compounds **1** and **3**, where the coloration efficiency values (CE > 200, **Table 2**) are promising for future structural optimization. On the other

hand, compound **4**, which presents slightly lower CE, possess the property of active shielding from UV-A light. Note that these results obtained in neat films well correlate with the behavior in solution (**Figure 5**) .

Table 2. Electrochromic properties of investigated compounds. λ – investigated wavelength; T_{ox} – transmittance of oxidized film at given wavelength λ; T_{red} – transmittance of neutral film at given wavelength λ; ΔOD – a difference of optical density between neutral and oxidized film at given wavelength λ; Q_D – charge density calculated in a chronoculometric experiment; CE – coloration efficiency; CR – contrast ratio. For further information please see previous works.[38–40]

Compound	**λ, nm (eV)**	**T_{ox}, %**	**T_{red}, %**	**ΔOD**	**Q_D, $mC \cdot cm^{-2}$**	**CE, $cm^2 \cdot C^{-1}$**	**CR (-)**
1	345 (3.59)	60.90	9.03	0.829	2.84	291.88	6.74
	408 (3.04)	18.56	86.52	0.669		235.40	4.66
2	340 (3.65)	67.61	26.39	0.408	2.62	155.94	2.56
	400 (3.10)	46.65	86.38	0.267		102.12	1.85
3	348 (3.56)	39.59	6.35	0.795	2.61	304.53	6.23
	417 (2.97)	28.16	73.18	0.415		158.91	2.60
4	306 (4.05)	73.18	28.16	0.415	3.17	130.84	2.60
	367 (3.37)	37.82	95.48	0.402		126.87	2.52

3.6 EPR

Electron Paramagnetic Resonance (EPR) spectroscopy gives a better insight into the radical species formed in solution than simple UV-Vis-NIR absorption measurement does. Through analysis of signal shift and structure, the localization of the unpaired electron density can be identified. All compounds but **1** give featureless EPR absorption that cannot be easily resolved (**Figure 7**, S6). **1** shows a visible hyperfine structure that can easily be spotted, yet the resolution is not high. The reason for it is most likely a strong delocalization of the radical and existence of multiple couplings with many nuclei. The cation radicals formed upon oxidation of **1** is showing a complex hyperfine structure. Assuming the oxidation should appear on the diarylamino group(s) the most simple model should comprise of N +xH nuclei, where x=2-6 due to the presence of two symmetric *N*-phenyl groups. Such a model, N + 4H gives a poor fit (**Figure 7**). While knowing the calculated HOMO

isosurfaces show that both donors are partly conjugated with each other through the acceptor group. It is possible for the radical to be delocalized over both donors. In this case, a model with two diarylamine units has to be used, i.e. (N^{I} + $4H^{I}$) + (N^{II} + $4H^{II}$). As shown in **Figure 7** the model with delocalization of the radical over two donor units fits the experimental spectrum very well. Similar *g*-factors are observed in cation radicals formed from molecules **2**−**4** (Table 3), therefore a similar nature of the paramagnetic species is to be expected. Especially that all molecules **1**−**4** show similarly equal contributions of both donors to the HOMO with a small contribution from the acceptor. Strong delocalization of the radical cations is in line with their expected nature as there occurr multiple couplings from the N and H nuclei in donor units as well as additional nuclei, such as H or N from the acceptor unit.

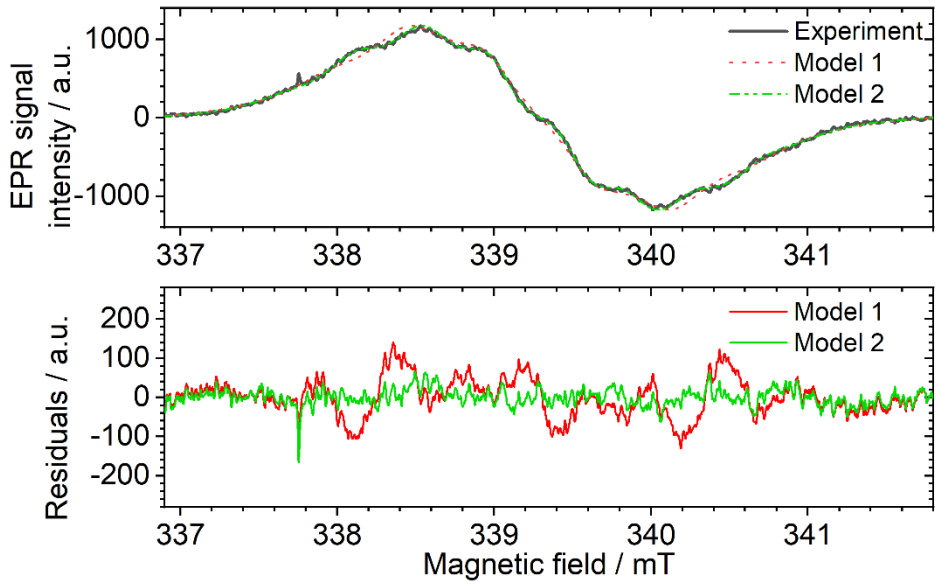

Figure 7. EPR spectrum of cation radicals formed upon *in situ* oxidation of **1** to the first oxidation potential. Model 1: 1N (0.20 mT); 4H (0.53 mT); Model 2: $1N^{I}$ (0.42 mT); $4H^{I}$ (0.18 mT); $1N^{II}$ (0.18 mT); $4H^{II}$ (0.08 mT).

Table 3. Giromagnetic factor (*g*-factor) of cation radicals formed by *in situ* oxidation of **1**−**4**.

	g-factor
1	2.0036
2	2.0037
3	2.0038
4	2.0038

3.7 Photophysics in a solid film

Fluorescence spectra of the studied acridone derivatives in Zeonex are in general similar to those obtained in toluene solutions (**Figure 8**). Molecules **1**−**3** show delayed fluorescence (DF) at 300 K with the spectrum collected at 20 ms delay being identical to the prompt fluorescence (nanosecond delay). In all of the delayed fluorescence spectra, a low energy shoulder or additional low energy peak can be seen. The contribution of this additional emission decreases at higher temperatures, i.e. from 300 to 320 K. Furthermore, at 80 K the delayed fluorescence is no longer dominating the delayed emission, and instead, at 20 ms delay, phosphorescence is observed. A comparison of phosphorescence spectra at 80 K with the low energy shoulder/peak suggests that phosphorescence is also present at temperatures around 300-320 K. On the other hand, low-temperature phosphorescence spectra of **1** and **3** reveal a high energy shoulder that coincides with prompt fluorescence spectrum, clearly indicating the existence of delayed fluorescence at low temperatures.

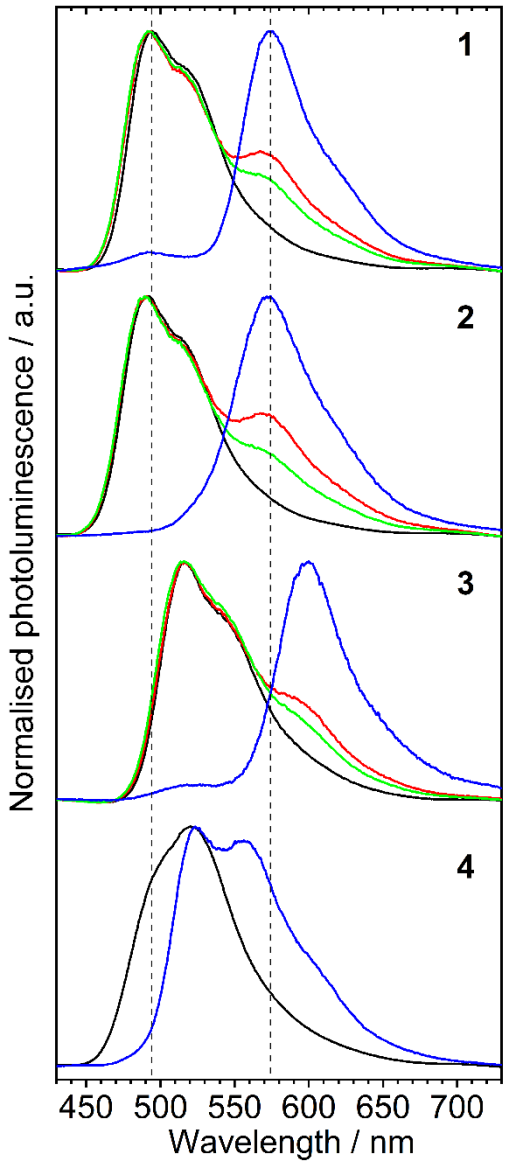

Figure 8. Prompt fluorescence (black line), delayed fluorescence at 20 ms delay (at 300 K – red line; at 320 K – green line), and phosphorescence at 20 ms delay at 80 K (blue line) in Zeonex 0.2 % (w/w) thin film. The phosphorescence spectrum of **4** was recorded at a 10 ms delay. The vertical dashed line is shown as an eye-guide for the maxima of prompt fluorescence and phosphorescence spectra of **1**.

Excited-state energy of **1**−**4** estimated from fluorescence and phosphorescence spectra onsets are summarised in **Table 4**. The singlet-triplet energy splitting, ΔE_{ST} in **1**−**3** is virtually identical, at 0.35−0.36 eV, but the value in **4** is only 0.16 eV. The lowest triplet excited state, T_1, in D-A-D molecules is often localized[41] on the part of the molecule, i.e. only the donor or acceptor, in contrary with the CT character of the S_1. Similarities in the shape of the phosphorescence spectrum of **1**−**3** may indicate localization of the T_1 at the same moiety. A previously studied[42] D-A-D molecule

with an *N*,*N*-dianisylamino donating group has shown T_1 at 2.21 eV, identical with the value obtained in **3**, which uses the same donor. The acceptor T_1 energy, in that case, was 2.40 eV, indicating the 2.21 eV value was likely related to the donor. The energy of T_1 in **1**−**4** series depends on the donor used and thus T_1 in **1**−**3** is likely to be located on the *N*,*N*-diarylamino unit. Consequently, in **4** T_1 is most likely to be located on acridone acceptor, as its T_1 energy coincides with the energy of the T_1 in **BCbAc**, attributed to the 2,6-substituted acridone acceptor (*N*-substituted acridone shows triplet energy of 2.8 eV[43]). Non-aromatic morpholine donor in **4** will have a high-lying n-σ* or σ-σ* T_1 due to lack of π electrons and thus the observed phosphorescence should be attributed to the acceptor rather than the donor.

Table 4. Photoluminescence properties of **1**−**4** in Zeonex thin film.

Compound	**τ_{PF}, ns[a]**	**τ_{TADF}, ms[b]**	**τ_{PH}, ms[c]**	**S_1, eV[d]**	**T_1, eV[e]**	**ΔE_{ST}, eV[f]**	**E_a, eV[g]**
1	30.2±0.3	98±6	200±40	2.68	2.32	0.36	0.24±0.01
2	15.3±0.5	95±3	300±60	2.70	2.35	0.35	0.21±0.01
3	36.2±0.9	79±8 (73%) 3.0±0.7 (27%) τ_{av} = 78±8	105±9	2.56	2.21	0.35	0.20±0.01
4	24.1±0.3	-	-	2.68	2.52	0.16	-

[a] Prompt fluorescence lifetime at 300 K; [b] TADF lifetime at 300 K; [c] phosphorescence lifetime at 80 K; [d] singlet state energy from fluorescence spectrum; [e] triplet state energy from phosphorescence spectrum at 80 K; [f] singlet-triplet energy gap; [g] TADF activation energy estimated from temperature-dependent spectra.

Photoluminescence decay of **1**−**4** in Zeonex is shown in **Figure 9**, while the decay constants are summarized in **Table 4**. All D-A-D molecules studied here show a fast prompt fluorescence component, with a decay lifetime in a range of 15-36 ns. **1**−**3** show a second decay component, with an emission spectrum identical to prompt fluorescence. This second component, with a lifetime of ≈80-100 ms is attributed to delayed fluorescence. The delayed fluorescence shows a visible temperature dependence (Figures S3 and S4), consistent with thermally activated delayed fluorescence. At temperatures below 200 K, the long-lived emission is dominated by phosphorescence which has a longer lifetime than TADF at RT: 105-300 ms. Given that the ΔE_{ST} in **4** is less than half of the value in the other emitters it seems not straightforward to explain why that

is not reflected on stronger TADF emission. Smaller ΔE_{ST} would normally promote TADF. However, small ΔE_{ST} is not the only requirement for TADF. In general, the T_1 decay through TADF should be faster than the radiative or non-radiative deactivation of T_1 directly to the ground state, S_0. It appears that in **4** the T_1 is too short-lived to support the TADF pathway, while long-lived (τ_{PH} > 100 ms) T_1 in **1**−**3** can do so. Finally, due to small signal intensity, phosphorescence decay of **4** could not be resolved.

Laser fluence experiment (Figure S5) shows a linear dependence of delayed fluorescence upon excitation power (energy per pulse) in **1** and **2** confirming its TADF mechanism. The power dependence of DF in **3** is supralinear with the power law of 1.38. While a power law of 1, or linear, proportional relation, identifies TADF, the value of 2 indicates triplet-triplet annihilation (TTA). A value of 1.38 does indicate that TADF is the main mechanism, but TTA is also present. The existence of two parallel mechanisms is evidenced by the biexponential character of the DF decay: the longer-lived component, $\tau_1 = 79 \pm 8$ ms, attributed to TADF and the shorter-lived, $\tau_2 = 3.0 \pm 0.7$ ms, attributed to TTA. The appearance of TTA in the solid film does not indicate i.e. that **3** is a less efficient TADF emitter, but TTA occurs due to close contacts between emitter molecules, i.e. related to some degree of aggregation. Interestingly, the occurrence of delayed fluorescence at 80 K despite relatively large ΔE_{ST}, as seen in **1**-**3**, is highly likely to be attributed to TTA. For an example, identical behavior has been observed previously in **BCbAc**.[20]

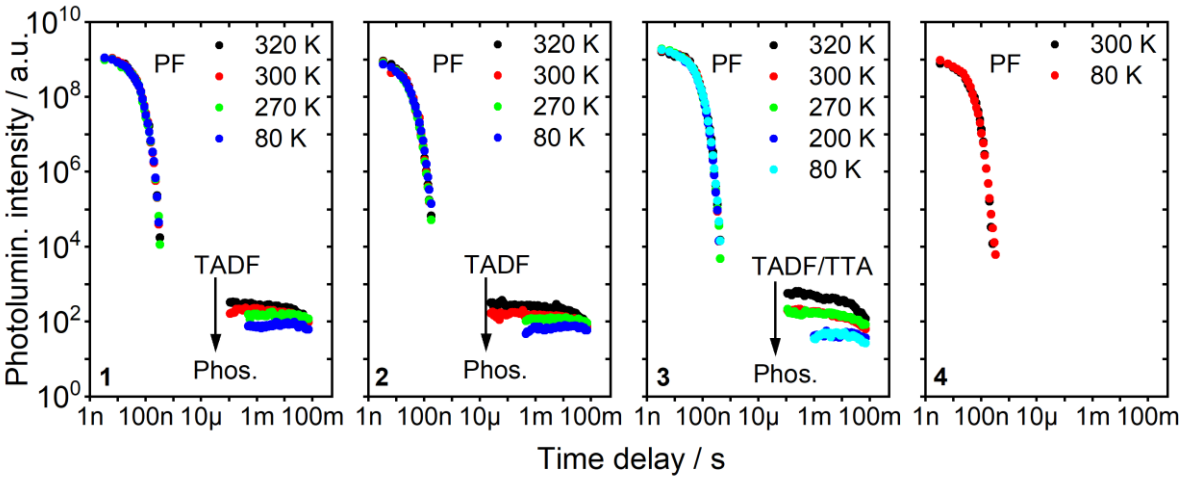

Figure 9. Photoluminescence decay of **1**−**4** in Zeonex 0.2% (w/w) thin film.

Finally, to understand the properties of **1**−**4** in OLED host, CBP, their photoluminescence decay (**Figure 10**) and time-resolved photoluminescence spectra (Figure S6) have been collected at 300 K. The behavior of molecules **1**−**4** (5%) in CBP is in agreement with their behavior in Zeonex. Only molecule **1** shows an additional decay component that is not present in Zeonex films. This medium-lived component is associated with TTA. This is justified by the higher concentration of molecules in OLED host than Zeonex, which promotes close contacts between emitter units.

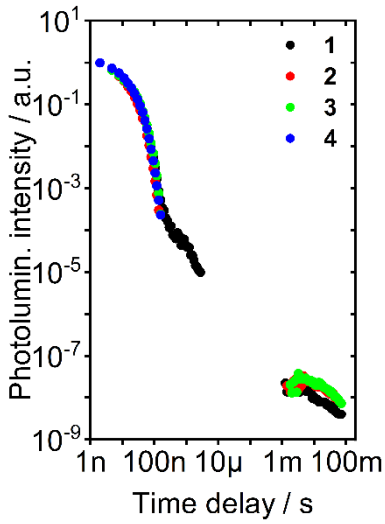

Figure 10. Photoluminescence decay of **1**−**4** in CBP 5% (w/w) thin film.

3.8 Electroluminescent devices

OLED devices were fabricated only using compounds **1-3** as the only to show clear TADF characteristics in CBP, later used as host in OLED devices. A device structure ITO | NPB(40 nm) | TSBPA(10 nm) | CBP co 5% **1-3** (20 nm) | TPBi (50 nm) | LiF (0.8 nm) | Al(100 nm) (Dev 1-3) was found to be initially the most successful for all three derivatives (**Table 5**, **Figure 11**). Having noticed some devices may suffer from re-absorption of electroluminescence by the emitter, we have fabricated another OLED using **1** at concentration reduced to 1.5 % (Dev 4). This device had a different structure than the previous Dev 1-3, comprising a blend host for improved charge balance: ITO | HAT-CN (10 nm) | TSBPA(40 nm) | mCP (2 nm) | mCP:PO-T2T (60:40) co 1.5% **1** (20 nm) | PO-T2T (50 nm) | LiF (0.8 nm) | Al(100 nm). Device turn-on voltage V_{ON} = 4.0 V of Dev 1 and 2 and 4.5 V in Dev 4 suggests a good alignment of energy levels, indicating no significant charge injection barriers. In Dev 3 the V_{ON} = 5.1 V is slightly higher, which is most likely related to the generally lower current density in this device. The maximum external quantum efficiency, $\eta_{ext., max}$, achieves the highest value for Dev 4, 5.4 %, and a minimum value of 1.8 % in Dev 3. Devices 1 and 2 show an exceptionally large luminance, above 20000 cd m^{-2}. The lower luminance of Dev 3 is a combination of both: lower device current and external quantum efficiency. The full width at half maximum (FWHM) remains in a range of 69-85 nm for devices 1-3, while it is even smaller, at 66 nm in Dev 4 (**Figure 12**). These figures are larger than the 53 nm recorded for **BCbAc**. This supposed broadening is caused by the fact that wavelength scale is not proportional to excited state energy, thus FWHM cannot be compared in emitters with different colors. Despite FWHM expressed in nm is still broadly used. If using energy scale instead, the FWHM appears to be much more consistent between the acridone-based emitters, with 300 meV in Dev 1 and 4 and 340 meV in Dev 2 and 3, compared with 290 meV in the **BCbAc**-based device. These values are very small in comparison with typical green CT emitters with usual broad emission, i.e. FWHM ≈ 600 meV.[3] The narrowest electroluminescence spectra of TADF emitters reach FWHM ≈ 170 meV or 28 nm in the blue

region.[28] Further comparison of electroluminescence spectra between Dev 1 and 4, comprising the same emitter shows the latter to be blue shifted in respect to the former. This apparent behaviour is caused by partial re-absorption of the electroluminescence by the emitting layer in Dev 1 which does not occur in Dev 4 due to a very low dopant concentration of only 1.5 %.

Table 5. Summary of electroluminescent properties of OLED devices Dev 1−4.

Device		**Dev 1**	**Dev 2**	**Dev 3**	**Dev 4**
Emitter		**1**	**2**	**3**	**1**
Doping concentration, %		5	5	5	1.5
V_{ON} (at 10 cd m^{-2}), V [a]		4.0	4.0	5.1	4.5
L_{max}, cd m^{-2} [b]		20800	22900	5900	9500
λ_{max}, nm [c]		516	508	543	509
CIE 1931 (x; y) [d]		0.30; 0.62	0.25; 0.57	0.41; 0.56	0.24; 0.55
FWHM, nm		69	72	85	66
$\eta_{L,\ max}$, cd A^{-1} [e]		11.9	8.0	5.6	11.1
$\eta_{ext.,\ max}$, % [f]		3.9	2.7	1.8	5.4
2 mA cm^{-2}	**η_L, cd A^{-1} [g]**	11.9	8.0	5.4	8.3
	$\eta_{ext.}$, % [h]	3.4	2.5	1.6	2.8
10 mA cm^{-2}	**η_L, cd A^{-1} [g]**	10.1	7.6	5.0	7.3
	$\eta_{ext.}$, % [h]	2.9	2.4	1.4	2.3
100 mA cm^{-2}	**η_L, cd A^{-1} [g]**	7.3	5.7	3.4	4.8
	$\eta_{ext.}$, % [h]	2.0	1.8	1.0	1.5

[a] turn-on voltage at 10 cd m^{-2}; [b] maximum luminance; [c] electroluminescence spectrum maxima; [d] color coordinates at maximum brightness as defined in International Commission on Illumination color space CIE 1931; [e] maximum current efficiency; [f] maximum external quantum efficiency; [g] current efficiency at specified current density; [g] external quantum efficiency at specified current density.

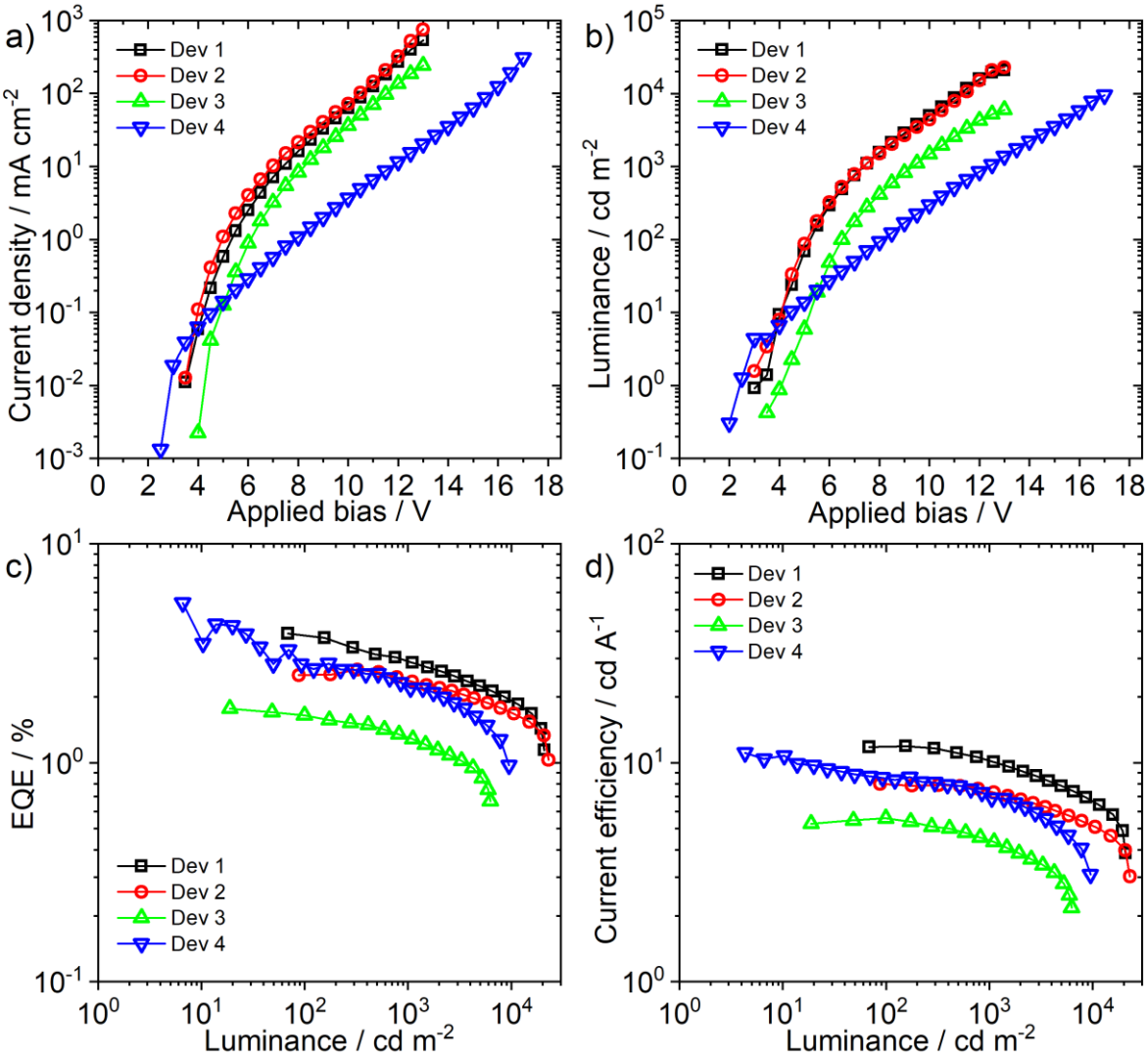

Figure 11. OLED device characteristics: a) current density – voltage characteristics; b) luminance – voltage characteristics; c) EQE *vs.* luminance; d) current efficiency *vs.* luminance.

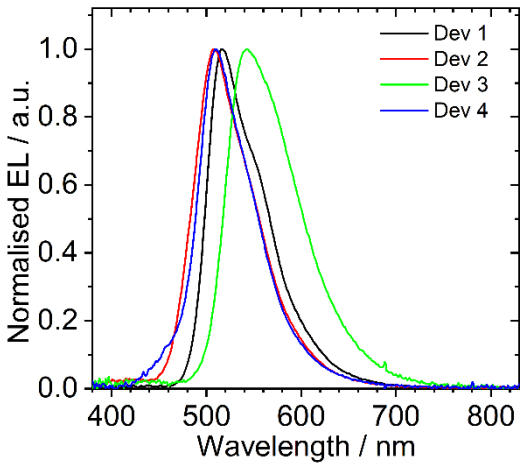

Figure 12. Electroluminescence spectra of devices Dev 1-4.

4 Conclusions

A group of acridone-amine D-A-D green emitters with a narrow photoluminescence spectrum and TADF properties has been demonstrated. The emitters have been used in bright OLED devices. The emitters have shown a prompt photoluminescence lifetime of 15-36 ns and a TADF lifetime of ≈ 90 ms. We present a relatively uncommon approach to achieve TADF by exploring the effect of a long-lived triplet state rather than aiming to reduce the ΔE_{ST}. Studying the presented D-A-D systems using spectroelectrochemical methods as well as calculations showed conjugation between the donor units and the acceptor. Such conjugation provides weak charge transfer properties of the excited state and provides a strategy to obtain a narrow photoluminescence spectrum in a TADF emitter. Electroluminescent devices presented in this work have shown luminance o up to 22900 cd m^{-2} (Dev 2) and EQE of up to 5.4 % (Dev 4). Furthermore, the presented acridone derivatives show excellent properties as electrochromic layers for potential application in UV-A / deep blue active shielding.

Conflicts of interests

There are no conflicts of interest to declare.

Acknowledgments

This work was supported by the EXCILIGHT project funded by the European Union's Horizon 2020 Research and Innovation Programme under grant agreement No. 674990. P.D. acknowledges the Polish National Science Centre funding, grant no. 2017/25/B/ST5/02488.

5 References

[1] C.W. Tang, S.A. VanSlyke, Organic electroluminescent diodes, Appl. Phys. Lett. 51 (1987) 913–915. https://doi.org/10.1063/1.98799.

[2] E. Longhi, L. De Cola, Iridium(III) Complexes for OLED Application, in: Iridium(III) Optoelectron. Photonics Appl., John Wiley & Sons, Ltd, Chichester, UK, 2017: pp. 205–274. https://doi.org/10.1002/9781119007166.ch6.

[3] Y. Tao, K. Yuan, T. Chen, P. Xu, H. Li, R. Chen, C. Zheng, L. Zhang, W. Huang, Thermally Activated Delayed Fluorescence Materials Towards the Breakthrough of Organoelectronics, Adv. Mater. 26 (2014) 7931–7958. https://doi.org/10.1002/adma.201402532.

[4] J.A.G. Williams, S. Develay, D.L. Rochester, L. Murphy, Optimising the luminescence of platinum(II) complexes and their application in organic light emitting devices (OLEDs), Coord. Chem. Rev. 252 (2008) 2596–2611. https://doi.org/10.1016/j.ccr.2008.03.014.

[5] B. Geffroy, P. le Roy, C. Prat, Organic light-emitting diode (OLED) technology: materials, devices and display technologies, Polym. Int. 55 (2006) 572–582. https://doi.org/10.1002/pi.1974.

[6] H. Yersin, Highly Efficient OLEDs with Phosphorescent Materials, Wiley, 2008.

[7] X. Yang, C. Yao, G. Zhou, Highly Efficient Phosphorescent Materials Based on Platinum Complexes and Their Devices (OLEDs), Platin. Met. Rev. 57 (2013) 2–16. https://doi.org/10.1595/147106713X659019.

[8] K.T. Kamtekar, A.P. Monkman, M.R. Bryce, Recent Advances in White Organic Light-Emitting Materials and Devices (WOLEDs), Adv. Mater. 22 (2010) 572–582. https://doi.org/10.1002/adma.200902148.

[9] F.B. Dias, K.N. Bourdakos, V. Jankus, K.C. Moss, K.T. Kamtekar, V. Bhalla, J. Santos, M.R. Bryce, A.P. Monkman, Triplet Harvesting with 100% Efficiency by Way of Thermally Activated Delayed Fluorescence in Charge Transfer OLED Emitters, Adv. Mater. 25 (2013) 3707–3714. https://doi.org/10.1002/adma.201300753.

[10] K.-H. Kim, S. Yoo, J. Kim, Boosting Triplet Harvest by Reducing Nonradiative Transition of Exciplex toward Fluorescent Organic Light-Emitting Diodes with 100% Internal Quantum Efficiency, Chem. Mater. 28 (2016) 1936–1941. https://doi.org/10.1021/acs.chemmater.6b00478.

[11] H. Uoyama, K. Goushi, K. Shizu, H. Nomura, C. Adachi, Highly efficient organic light-emitting diodes from delayed fluorescence, Nature. 492 (2012) 234–238. https://doi.org/10.1038/nature11687.

[12] Z. Yang, Z. Mao, Z. Xie, Y. Zhang, S. Liu, J. Zhao, J. Xu, Z. Chi, M.P. Aldred, Recent advances in organic thermally activated delayed fluorescence materials, Chem. Soc. Rev. 46 (2017) 915–1016. https://doi.org/10.1039/C6CS00368K.

[13] H. Noda, R. Kabe, C. Adachi, Blue Thermally Activated Delayed Fluorescence Molecule Having Acridan and Cyanobenzene Units, Chem. Lett. (2016) cl.160814. https://doi.org/10.1246/cl.160814.

[14] C. Adachi, Third-generation organic electroluminescence materials, Jpn. J. Appl. Phys. 53 (2014) 0–11. https://doi.org/10.7567/JJAP.53.060101.

[15] M. Li, Y. Liu, R. Duan, X. Wei, Y. Yi, Y. Wang, C.F. Chen, Aromatic-Imide-Based Thermally Activated Delayed Fluorescence Materials for Highly Efficient Organic Light-Emitting Diodes, Angew. Chemie - Int. Ed. 56 (2017) 8818–8822. https://doi.org/10.1002/anie.201704435.

[16] H.F. Higginbotham, P. Pander, R. Rybakiewicz, M.K. Etherington, S. Maniam, M. Zagorska, A. Pron, A.P. Monkman, P. Data, Triphenylamine disubstituted naphthalene diimide: elucidation of excited states involved in TADF and application in near-infrared organic light emitting diodes, J. Mater. Chem. C. 6 (2018) 8219–8225. https://doi.org/10.1039/C8TC02936A.

[17] V. Cherpak, P. Stakhira, B. Minaev, G. Baryshnikov, E. Stromylo, I. Helzhynskyy, M. Chapran, D. Volyniuk, Z. Hotra, A. Dabuliene, A. Tomkeviciene, L. Voznyak, J.V. Grazulevicius, Mixing of Phosphorescent and Exciplex Emission in Efficient Organic Electroluminescent Devices, ACS Appl. Mater. Interfaces. 7 (2015) 1219–1225. https://doi.org/10.1021/am507050g.

[18] D. Kourkoulos, C. Karakus, D. Hertel, R. Alle, S. Schmeding, J. Hummel, N. Risch, E. Holder, K. Meerholz, Photophysical properties and OLED performance of light-emitting platinum(ii) complexes, Dalt. Trans. 42 (2013) 13612. https://doi.org/10.1039/c3dt50364j.

[19] P. Pander, R. Bulmer, R. Martinscroft, S. Thompson, F.W. Lewis, T.J. Penfold, F.B. Dias, V.N. Kozhevnikov, 1,2,4-Triazines in the synthesis of bipyridine bisphenolate onno ligands and their highly luminescent tetradentate pt(II) complexes for solution-processable oleds, Inorg. Chem. 57 (2018) 3825–3832. https://doi.org/10.1021/acs.inorgchem.7b03175.

[20] P. Pander, A. Swist, R. Motyka, J. Soloducho, F.B. Dias, P. Data, Thermally activated delayed fluorescence with a narrow emission spectrum and organic room temperature phosphorescence by controlling spin–orbit coupling and phosphorescence lifetime of metal-free organic molecules, J. Mater. Chem. C. 6 (2018) 5434–5443. https://doi.org/10.1039/C8TC00175H.

[21] R. Liu, G. Zhu, G. Zhang, N-Substitution of acridone with electron-donating groups: crystal packing, intramolecular charge transfer and tuneable aggregation induced emission, RSC Adv. 10 (2020) 7092–7098. https://doi.org/10.1039/C9RA10615D.

[22] I. Kulszewicz-Bajer, M. Zagorska, M. Banasiewicz, P.A. Guńka, P. Toman, B. Kozankiewicz, G. Wiosna-Salyga, A. Pron, Effect of the substituent position on the electrochemical, optical and structural properties of donor-acceptor type acridone derivatives, Phys. Chem. Chem. Phys. 22 (2020) 8522–8534. https://doi.org/10.1039/d0cp00521e.

[23] Q.T. Siddiqui, A.A. Awasthi, P. Bhui, M. Muneer, K.R.S. Chandrakumar, S. Bose, N. Agarwal, Thermally Activated Delayed Fluorescence (Green) in Undoped Film and Exciplex Emission (Blue) in Acridone–Carbazole Derivatives for OLEDs, J. Phys. Chem. C. 123 (2019) 1003–1014. https://doi.org/10.1021/acs.jpcc.8b08357.

[24] P. Pander, A. Swist, P. Zassowski, J. Soloducho, M. Lapkowski, P. Data, Electrochemistry and spectroelectrochemistry of polymers based on D-A-D and D-D-D bis(N-carbazolyl) monomers, effect of the donor/acceptor core on their properties, Electrochim. Acta. 257 (2017) 192–202. https://doi.org/10.1016/j.electacta.2017.10.023.

[25] B. Weniger, B.-H. Um, A. Valentin, A. Estrada, A. Lobstein, R. Anton, M. Maillé, M. Sauvain,

Bioactive Acridone Alkaloids from Swinglea g lutinosa, J. Nat. Prod. 64 (2001) 1221–1223. https://doi.org/10.1021/np0005762.

[26] P.L. dos Santos, M.K. Etherington, A.P. Monkman, Chemical and conformational control of the energy gaps involved in the thermally activated delayed fluorescence mechanism, J. Mater. Chem. C. 6 (2018) 4842–4853. https://doi.org/10.1039/C8TC00991K.

[27] T. Huang, W. Jiang, L. Duan, Recent progress in solution processable TADF materials for organic light-emitting diodes, J. Mater. Chem. C. 6 (2018) 5577–5596. https://doi.org/10.1039/C8TC01139G.

[28] T. Hatakeyama, K. Shiren, K. Nakajima, S. Nomura, S. Nakatsuka, K. Kinoshita, J. Ni, Y. Ono, T. Ikuta, Ultrapure Blue Thermally Activated Delayed Fluorescence Molecules: Efficient HOMO-LUMO Separation by the Multiple Resonance Effect, Adv. Mater. 28 (2016) 2777–2781. https://doi.org/10.1002/adma.201505491.

[29] B.K. Sharma, A.M. Shaikh, N. Agarwal, R.M. Kamble, Synthesis, photophysical and electrochemical studies of acridone-amine based donor–acceptors for hole transport materials, RSC Adv. 6 (2016) 17129–17137. https://doi.org/10.1039/C5RA25115J.

[30] F. Neese, Software update: the ORCA program system, version 4.0, WIREs Comput. Mol. Sci. 8 (2018). https://doi.org/10.1002/wcms.1327.

[31] F. Neese, The ORCA program system, WIREs Comput. Mol. Sci. 2 (2012) 73–78. https://doi.org/10.1002/wcms.81.

[32] A.-R. Allouche, Gabedit-A graphical user interface for computational chemistry softwares, J. Comput. Chem. 32 (2011) 174–182. https://doi.org/10.1002/jcc.21600.

[33] A.D. Becke, Density-functional thermochemistry. III. The role of exact exchange, J. Chem. Phys. 98 (1993) 5648–5652. https://doi.org/10.1063/1.464913.

[34] P.J. Stephens, F.J. Devlin, C.F. Chabalowski, M.J. Frisch, Ab Initio Calculation of Vibrational Absorption and Circular Dichroism Spectra Using Density Functional Force Fields, J. Phys. Chem. 98 (1994) 11623–11627. https://doi.org/10.1021/j100096a001.

[35] W.J. Hehre, R. Ditchfield, J.A. Pople, Self—Consistent Molecular Orbital Methods. XII. Further Extensions of Gaussian—Type Basis Sets for Use in Molecular Orbital Studies of Organic Molecules, J. Chem. Phys. 56 (1972) 2257–2261. https://doi.org/10.1063/1.1677527.

[36] P. Pander, P. Data, F.B. Dias, Time-resolved Photophysical Characterization of Triplet-harvesting Organic Compounds at an Oxygen-free Environment Using an iCCD Camera, J. Vis. Exp. (2018). https://doi.org/10.3791/56614.

[37] D. de Sa Pereira, A.P. Monkman, P. Data, Production and Characterization of Vacuum Deposited Organic Light Emitting Diodes, J. Vis. Exp. (2018). https://doi.org/10.3791/56593.

[38] P. Pander, R. Motyka, P. Zassowski, M. Lapkowski, A. Swist, P. Data, Electrochromic Properties of Novel Selenophene and Tellurophene Derivatives Based on Carbazole and Triphenylamine Core, J. Phys. Chem. C. 121 (2017) 11027–11036. https://doi.org/10.1021/acs.jpcc.7b00216.

[39] H.F. Higginbotham, M. Czichy, B.K. Sharma, A.M. Shaikh, R.M. Kamble, P. Data, Electrochemically synthesised xanthone-cored conjugated polymers as materials for electrochromic windows, Electrochim. Acta. 273 (2018) 264–272.

https://doi.org/10.1016/j.electacta.2018.04.070.

[40] S. Pluczyk, M. Vasylieva, P. Data, Using Cyclic Voltammetry, UV-Vis-NIR, and EPR Spectroelectrochemistry to Analyze Organic Compounds, J. Vis. Exp. (2018) e56656. https://doi.org/10.3791/56656.

[41] F.B. Dias, J. Santos, D.R. Graves, P. Data, R.S. Nobuyasu, M.A. Fox, A.S. Batsanov, T. Palmeira, M.N. Berberan-Santos, M.R. Bryce, A.P. Monkman, The Role of Local Triplet Excited States and D-A Relative Orientation in Thermally Activated Delayed Fluorescence: Photophysics and Devices, Adv. Sci. 3 (2016) 1600080. https://doi.org/10.1002/advs.201600080.

[42] P. Data, P. Pander, M. Okazaki, Y. Takeda, S. Minakata, A.P. Monkman, Dibenzo[a,j]phenazine-Cored Donor-Acceptor-Donor Compounds as Green-to-Red/NIR Thermally Activated Delayed Fluorescence Organic Light Emitters, Angew. Chemie Int. Ed. 55 (2016) 5739–5744. https://doi.org/10.1002/anie.201600113.

[43] D. a K. Vezzu, J.C. Deaton, M. Shayeghi, Y. Li, S. Huo, Acridinone/Amine(carbazole)-Based Bipolar Molecules: Efficient Hosts for Fluorescent and Phosphorescent Emitters, Org. Lett. 11 (2009) 4310–4313. https://doi.org/10.1021/ol901584g.